On the feasibility of large-aperture Fresnel lenses for the microfocusing of hard X-rays

Werner Jark,* Fréderic Pérennès and Marco Matteucci

Sincrotrone Trieste ScpA, SS 14 km 163.5, 34012 Basovizza (TS), Italy.
E-mail: werner.jark@elettra.trieste.it

Like visible light, X-rays can also be focused by refraction in transmission lenses. For visible light this requires convex lenses while for X-rays one needs to use concave lenses instead. Both lens types can be lightened by the material removal strategy introduced by Fresnel, which results in a lens subdivided into zones. Until now, for the focusing of X-rays, stacks of standard lenses and of Fresnel lenses have mostly been produced. The first are dubbed compound refractive lenses, abbreviated as CRL. State-of-the-art systems of this kind now achieve almost theoretical performance for the focus size and the transmission. On the other hand, the latter Fresnel systems, which promise to provide larger apertures, are still in their infancy. This report discusses systematically the properties of two possible schemes for their realisation. It then compares the optimized apertures of these two schemes with those for CRLs. The best Fresnel lenses in this study are found to provide experimentally more than 50% of the expected refraction efficiency at 8.5 keV photon energy. The photon flux in their focus is then almost identical to that of perfect Be CRLs with the same focal length. This report will also interpret experimental data reported previously for other Fresnel lenses.

1. Introduction

G. W. Roentgen realised immediately after his discovery of X-rays in 1895 that they were not deflected appreciably by matter. Consequently the construction of optics, and in particular of transmission lenses, for focusing X-rays seemed to be impossible. Kirkpatrick & Baez (1948) confirmed that the focal length even for stacks of refractive transmission lenses would be unpractical numbers of the order of 100 m. It was only after the introduction of third-generation synchrotron radiation sources that Suehiro et al. (1991) finally identified an application for X-ray lenses with very long focal lengths. As these lenses have to be concave in shape, the off-axis increasing absorption will limit the useful aperture; Suehiro et al. (1991) have already discussed the use of the Fresnel variant, which they consider to be feasible using a lathe. Michette (1991) comments on this latter study critically. Nevertheless, Yang (1993) systematically discussed the use and the technical feasibility of refractive X-ray lenses, especially of the Fresnel version. Finally, Tomie (1994) received patent protection for the production of concave refractive X-ray lenses. The material left between many small drilled holes, which are aligned in a line, forms a stack of cylindrical bi-concave lenses. These lenses focus in only one direction, and thus for bi-dimensional focusing one needs to align two

systems following each other with orthogonal holes. The first prototype of such a system was operated by Snigirev et al. (1996). These lenses were given the name compound refractive lenses. Lengeler et al. (2004) improved the shape and the production process for such lenses, which now have parabolic and rotationally symmetric surfaces. These lenses focus bi-dimensionally and can be produced in the low-absorbing beryllium. The recently measured transmission and spatial resolution are almost in agreement with the predictions. Aristov et al. (2000) produced the first prototype of the concave Fresnel lens as a stack of five lenses with identical shape using deep X-ray lithography. This production process does not allow rotationally symmetric lenses to be made and thus the prototypes are once more linear systems. More of these lenses were produced recently by Snigireva et al. (2001), Nöhammer et al. (2003), Evans-Lutterodt et al. (2003) and Nazmov et al. (2004). However, for none of them was a spatial resolution close to the diffraction limit verified. Jark et al. (2004) introduced a second variant of the Fresnel lens, which could be considered as the Fresnel version of the prism array lens invented by Cederström et al. (2000). The latter lens is composed of two identical lens halves of sawtooth profile, which are arranged as an open alligator mouth. This lead Dufresne et al. (2001) to call these objects alligator lenses. The removal of the optically passive material from this prism array

leads to a configuration of many small prisms of identical shape. The most compact arrangement for these segments in two large prisms was studied by Jark *et al.* (2004), giving the lens the shape of an hourglass. The Italian translation of the latter, clessidra, will be used here as the acronym for this Fresnel lens.

In this paper we will derive the theoretical transmission characteristics of all presented lenses. As the Fresnel lenses can only be produced as one-dimensionally focusing objects, the discussion will be restricted to this case. Then the bi-dimensionally focusing system will be composed of two crossed lenses, in which the apertures and the feature depths have to match. Consequently the production limits for the latter matching criterion will be taken into account in our discussion whenever necessary. We will try to identify optimum parameters such that the apertures of the different systems can be compared directly. This comparison will be based on the effective aperture of an optical system introduced by Lengeler *et al.* (1999), which is the equivalent aperture of a slit system that directs the same photon flux into the image. It will be investigated whether the spectral resolving power of standard monochromators for synchrotron radiation limits the diffraction-limited spatial resolution of these lenses. In addition, aperture limits will be derived up to which the lenses can be described as 'thin lenses'. In the experimental part we will compare the transmission characteristics, *i.e.* the transmission and the refraction efficiency, of some clessidras with the expectations. This will allow us to comment on the quality of the single segments in lenses produced in different photoresists. Finally we will investigate whether similar comments can be derived from the experimental data published for standard Fresnel lenses. It will be discussed how far the image size and the experimental refraction efficiency depend on the amount of spatially coherently illuminated rows in the lenses. The present discussion will only deal with lens systems that are based on highly regular and repeatable structures, which can be easily mass-produced. Their measured and expected performance will thus not be compared with that of other custom-made unique and expensive objects. In fact, Fresnel zone-plates (Yun *et al.*, 1999), two-dimensional waveguides (Jarre *et al.*, 2005) and state-of-the-art mirror optics (Hignette *et al.*, 2003; Mimura *et al.*, 2004) have already provided better performance for the measured spatial resolution. However, recently Schroer & Lengeler (2005) showed that adiabatically focusing Fresnel lenses may provide superior spatial resolution with an ultimate limit of the order of 2 nm. As this was carried out for lens parameters which are currently not within reach of state-of-the-art technology, this version of the Fresnel lens will not be discussed here further.

2. Theoretical considerations

2.1. Effective aperture

The parameter which allows the objective comparison of the collection area of optical systems is the effective aperture (Lengeler *et al.*, 1999), obtained by integrating the lens transmission function over the geometrical apertures,

$$A_{\text{eff}} = \int_{y_1}^{y_2} T(y) \, \mathrm{d}y. \qquad (1)$$

This equation can also be written as

$$A_{\text{eff}} = \bar{t} A_{\text{geo}}, \qquad (2)$$

where

$$A_{\text{geo}} = y_2 - y_1 \qquad (3)$$

is the geometrical aperture and

$$\bar{t} = \frac{\int t(y) \, \mathrm{d}y}{\int \mathrm{d}y} \qquad (4)$$

is the average transmission in the aperture. In order to facilitate the comparison in the present discussion we will define the optimum aperture A_{opt}, which is the geometrical aperture of a system A_{geo} for which the average transmission according to (4) becomes $\bar{t} \simeq 0.75$. This leads simply to

$$A_{\text{eff}} = 0.75 A_{\text{opt}}. \qquad (5)$$

All systems are considered to be symmetric around the optical axis at $y = 0$, where they are assumed to provide $t(y = 0) = 1$.

2.1.1. Compound refractive lenses. The surfaces of a one-dimensionally focusing symmetric concave transmission lens of parabolic shape, as shown in Fig. 1(*a*), are described by (the *x*-axis is the optical axis of the lens)

$$y^2 = \begin{cases} 2Rx & x > 0 \\ -2Rx & x < 0 \end{cases}, \qquad (6)$$

where R is the radius of curvature in the lens centre with $y = 0$. The focal length f of a stack of N identical bi-concave lenses is then given by (Snigirev *et al.*, 1996)

(a)   (b)

(c)   (d)   (e)
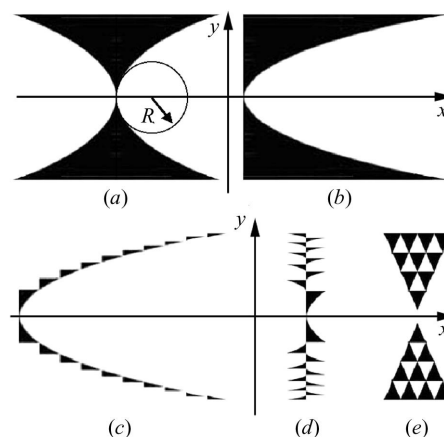
Figure 1
Possible schemes for refractive transmission lenses for the focusing of X-rays. (*a*) and (*b*) show a double concave and a plane concave lens of parabolic shape. (*c*) is the standard Fresnel lens obtained directly from (*b*), while (*d*) is a compacted design. (*e*) is the concept for the present clessidra prism lens. All lenses are drawn to scale for identical focal length. R is the radius of curvature of the lens surface in its centre as shown in (*a*).

$$f = R/2N\delta. \tag{7}$$

Here, δ is the unit decrement of the refractive index n of the material, which for X-rays is usually written as $n = 1 - \delta + i\beta$. For a mixture, δ is given by (Henke et al., 1993)

$$\delta = \left(r_e \lambda^2/2\pi\right) \sum_i N_i f_{1,i}, \tag{8}$$

where $r_e = 2.818 \times 10^{-15}$ m is the classical electron radius, λ is the wavelength and N_i is the number of atoms of a particular element i per unit volume, while $f_{1,i}$ is the related element-specific atomic scattering factor, which is tabulated by Henke et al. (1993) and by Chantler et al. (2003). Wavelength λ and photon energy E are related via $\lambda E = 1239.852$ nm eV.

For the standard bi-concave lens without material on the optical axis we find, according to Cederström et al. (2000), with (6) and (7),

$$t_{CRL}(y) = \exp(-2x/L) = \exp\left(-y^2/2\delta L f\right). \tag{9}$$

Here, L is the attenuation length of the material, which is also tabulated (Henke et al., 1993; Chantler et al., 2003). The present transmission function is of Gaussian shape, which leads to an average transmission of 0.747 in the optimum geometrical aperture,

$$A_{CRL,opt} = 2(2\delta L)^{1/2} f^{1/2}. \tag{10}$$

This aperture already transmits 84% of the ultimately transmittable photon flux by use of a larger aperture. The ultimately possible effective aperture for a larger lens is then

$$A_{CRL,eff,max} = (2\pi\delta L)^{1/2} f^{1/2} = 0.886 A_{CRL,opt}. \tag{11}$$

Note that the production process may require leaving some material, with total thickness d, on the lens optical axis. Then the average lens transmission will be reduced and equations (9) and (11) need to be multiplied by $\exp(-d/L)$.

2.1.2. Fresnel lenses. The strategy in Fresnel lenses is to remove absorbing but otherwise optically passive material from the thicker parts of the lens. This can be done, according to Suehiro et al. (1991), without distortion of the passing wavefront by removing blocks which retard or advance the phase of the transmitted wave by integer multiples p of 2π. The corresponding material thickness in the beam direction, D, is given by

$$D = p\lambda/\delta. \tag{12}$$

The plane concave lens in Fig. 1(b) permits the simplest description of the material removal strategy. Indeed, this lens shape was the starting point for all tested Fresnel lenses. In the lens in Fig. 1(b) one can remove a block of material of length D starting at any y for which one has $x = D$. For the lens optimization the parameter p will be more conveniently written as $p = km$, where k is an 'order number' and m is the 'step index'.

Standard Fresnel lens. The natural solution for a Fresnel lens with minimal absorption is achieved for $k = 1$ and when m is increased between steps by 1, which is the case for the lens in Fig. 1(c). This lens then has a constant zone width in the direction of the passing beam. The single lenses in the lens

stack of Aristov et al. (2000) had this shape. Later, Nöhammer et al. (2003) also used this shape in lens stacks and in single lenses. Evans-Lutterodt et al. (2003) obtained a similar shape for a single lens starting from the elliptical lens shape, which is better suited for creating a demagnified source image by use of a single lens. The single lens can be compacted as shown in Fig. 1(d), which then leads to shorter lens stacks as presented by Snigireva et al. (2001). The more recent lenses of Nazmov et al. (2004) are thus based on this concept. As far as the absorption is concerned, no further optimization of this concept is possible. The maximum amount of material in the remaining segments is $D' = \lambda/\delta$, while more generally it is

$$D' = k\lambda/\delta. \tag{13}$$

For a discussion on the transmission of the lens, we will approximate the remaining segments with triangles. Then the averaged optical path in the segments is $D'/2$. The average transmission in the segments of a stack of N_{Fr} identical lenses is constant in the lens aperture and approximately given by (the index Fr refers to this lens as a Fresnel lens)

$$\bar{t}_{Fr}(y) = \exp(-N_{Fr} k_{Fr} \lambda/2\delta L). \tag{14}$$

With the use of the focal length of $f = R/N\delta$ for a plane concave lens the steps occur at

$$y_{m,Fr} = (2N_{Fr} m_{Fr} k_{Fr} \lambda f)^{1/2}. \tag{15}$$

The geometrical aperture for a given number of steps m_{Fr} is then $A_{Fr,geo} = 2y_{m,Fr}$ and thus

$$A_{Fr,geo} = 2(2N_{Fr} m_{Fr} k_{Fr} \lambda)^{1/2} f^{1/2}. \tag{16}$$

The total number of segments in the lens is given by

$$M_{Fr} = 2N_{Fr} m_{Fr}. \tag{17}$$

For larger m_{Fr} the height of the mth step between m and $m - 1$ is approximately given by

$$\Delta y_{m,Fr} = A_{Fr,geo}/4m_{Fr}. \tag{18}$$

From this one can derive for the outermost segment in the lens,

$$\Delta y_{m,Fr} A_{Fr,geo} = 2N_{Fr} k_{Fr} \lambda f. \tag{19}$$

For $N_{Fr} = 1$, the latter two relations describe the properties for Fresnel phase-zone plates (Attwood, 1999). For fixed $A_{Fr,geo}$ and f and for a given k_{Fr} and λ we see from (19) that the size of the last segment $\Delta y_{m,Fr}$ increases linearly with the amount of lenses N_{Fr} in the stack. Consequently one can increase the segment size $\Delta y_{m,Fr}$ by increasing N_{Fr} at the expense of reduced transmission. According to (16) and (17) the number of segments in the lens does not change in this case.

The earlier-mentioned average transmission of 0.75 then leads with (14) to the optimum number of lenses $N_{Fr,opt}$ given by

$$N_{Fr,opt} = -2(\ln 0.75)\delta L/k_{Fr} \lambda = 0.575 \delta L/k_{Fr} \lambda. \tag{20}$$

Then the corresponding optimum geometrical aperture according to (16) can be written as

$$A_{\text{Fr,opt}} = 2(1.15m_{\text{Fr}})^{1/2} (\delta L)^{1/2} f^{1/2}, \quad (21)$$

which is independent of the order number k_{Fr}. The row index m_{Fr} remains at this point a still freely adjustable number.

Prism-type Fresnel lens – clessidras. The prism-type Fresnel lens clessidra introduced by Jark *et al.* (2004) is shown in Fig. 1(*e*). This new lens is intended to be used as a single lens, *i.e.* with $N_{\text{Cl}} = 1$. Most of the segments in this lens are prisms of identical size and shape, and only a few of the prism side-walls are curved in order to make the lens focus free of aberrations. In Fig. 1(*e*) this correction is made in the external side-walls. In this lens the index m_{Cl} refers to the row number as well as to the number of small prism-like objects in it. The total number of segments in a symmetric lens is then simply

$$M_{\text{Cl}} = m_{\text{Cl}}^2. \quad (22)$$

Also in this lens the base length of the single prisms, *i.e.* its material thickness in the beam direction, D, is given by $D' = k_{\text{Cl}}\lambda/\delta$. Then in this lens the average amount of material per row is linearly increasing with distance from the optical axis. Thus the transmission $t(y)$ decreases with increasing y. The step position can still be obtained from (15). However, in this case the step index m to be used is related to the row index m_{Cl} for the clessidra lens *via*

$$m = (m_{\text{Cl}} + 1)m_{\text{Cl}}/2. \quad (23)$$

For $m_{\text{Cl}} = 1$ we also find that $m = 1$ and thus from (15) we obtain

$$y_{m=1,\text{Cl}} = (2k_{\text{Cl}}\lambda f)^{1/2}. \quad (24)$$

For large m_{Cl} ($\gg 1$) the prism row borders are found approximately at

$$y_{m,\text{Cl}} \simeq m_{\text{Cl}}(k_{\text{Cl}}\lambda f)^{1/2}, \quad (25)$$

which leads to the constant step height

$$\Delta y_{m,\text{Cl}} \simeq (k_{\text{Cl}}\lambda f)^{1/2}. \quad (26)$$

For this lens type the focal length can thus be calculated for any material simply from the step height $\Delta y_{m,\text{Cl}}$ of the lens according to (26) as

$$f = \Delta y_{m,\text{Cl}}^2/k_{\text{Cl}}\lambda. \quad (27)$$

The average transmission of row m_{Cl} is now given in the triangle approximation by

$$t_{\text{Cl}}(y) = \exp[-m_{\text{Cl}}(y)\, k_{\text{Cl}}\lambda/2\delta L]. \quad (28)$$

The optimum row index, which leads to $\bar{t} = 0.75$, is then

$$m_{\text{Cl,opt}} = 1.212\, \delta L/k_{\text{Cl}}\lambda, \quad (29)$$

and the optimum geometrical aperture becomes

$$A_{\text{Cl,opt}} = 2.424\, \delta L(k_{\text{Cl}}\lambda)^{-1/2} f^{1/2}. \quad (30)$$

For a better direct comparison to (21) one can also write

$$A_{\text{Cl,opt}} = 2(1.212m_{\text{Cl}})^{1/2}(\delta L)^{1/2} f^{1/2}. \quad (31)$$

Note that here m_{Cl} is no longer a free parameter. The optimum aperture $A_{\text{Cl,opt}}$ transmits 45% of the ultimately transmittable photon flux for this kind of lens. It needs a 3.8-fold increase in the geometrical aperture in order to double the photon flux in the focus.

Correlations between the Fresnel lenses. In order to compare the optimum properties of all lenses with each other, we will now discuss briefly the correlations which exist between the two different variants of the Fresnel lenses for the same order, *i.e.* for $k_{\text{Fr}} = k_{\text{Cl}}$. From (20) and (29) we obtain

$$m_{\text{Cl,opt}} = 2.1\, N_{\text{Fr,opt}}. \quad (32)$$

Then in the optimum standard Fresnel lenses the number of lenses in the stack is about half of the number of rows in the clessidra, independent of the aperture of the first system. Now we will fix the previously free parameter m_{Fr} in (21) such that both lens variants have the same aperture. For this condition one can easily show that both lenses contain the same number of segments according to (17) and (22) and approximately the same number of rows. Then we will define the half-aperture of a lens, which is the axially symmetric aperture with half the size of the optimum lens aperture. At the border of this half-aperture both lenses have the same segment height and contain the same number of segments per row. Within this half-aperture the segments of the standard Fresnel lens are larger than those in the clessidra, while they are smaller outside. For both lenses the half-aperture comprises one-quarter of the total number of segments. Then only one-quarter of the segments in the standard Fresnel lens are larger than those in the clessidra and they fill the internal half-aperture, where the clessidra is more transparent. The remaining three-quarters of the segments are smaller than those in the clessidra and fill the external half-aperture, where now the standard Fresnel lens is more transparent than the clessidra. At the border of the lenses the segment height Δy_{Fr} in the standard Fresnel lens is only about half of the height of the clessidra segments Δy_{Cl}.

2.2. Bandwidth of refractive lenses

Up to this point we have completely ignored the fact that the incident X-ray radiation will have a finite spectral bandwidth $\Delta\lambda$. Now the present study deals with refractive lenses, in which the focal length depends on δ according to (7). According to (8), above the absorption edges, where the atomic scattering factors f_1 are constant, δ changes rapidly with wavelength, $\delta \propto \lambda^2$, and thus refractive lenses will necessarily suffer from chromatic aberrations. The refraction angle $\alpha(y)$ at a given position y in the lens is proportional to δ, which leads to the relation

$$\Delta\alpha(y)/\alpha(y) = 2\Delta\lambda/\lambda. \quad (33)$$

The deflection angle in the lens aperture at an off-axis distance y is given by $\alpha = y/f$. The angular spread of the transmitted radiation instead leads to a broadened image of size s in the focal plane of about $s = \Delta\alpha(y)f$. For simplicity we will assume here constant transmission in the optimum lens apertures.

Then the average for the ratio $\Delta\alpha/\alpha$ is given by $\overline{\Delta\alpha(y)}/\alpha(y) = 2s/A_{\mathrm{opt}}$. This puts an upper limit on the image blurring due to chromatic aberrations of

$$s_{\mathrm{chr}} = A_{\mathrm{opt}}\Delta\lambda/\lambda. \tag{34}$$

This is a surprisingly simple relation, which permits us to estimate rapidly the spatial resolution obtainable with a beam of finite bandwidth. The limiting case is the lens operation with diffraction-limited spatial resolution (Born & Wolf, 1980). In general this resolution applies to the minimum feature size that is detectable in the image produced by the lens. A special case is where the source is demagnified to the same size, which allows us then to obtain the same spatial resolution in a scanning instrument. Now the diffraction-limited spatial resolution s_{diff} for a one-dimensionally focusing object is given by

$$s_{\mathrm{diff}} = 1.45\lambda/2[\mathrm{NA}], \tag{35}$$

where [NA] is the numerical aperture of the lens (Born & Wolf, 1980). For constant transmission of the lens in the geometrical aperture we have $2[\mathrm{NA}] = A_{\mathrm{Cl,opt}}/f$. With $s_{\mathrm{chr}} = s_{\mathrm{diff}}$ we then obtain for the monochromaticity of the incident radiation, here expressed as the spectral resolving power $\lambda/\Delta\lambda$, the minimum request

$$\lambda/\Delta\lambda\,\big|^{\mathrm{chrom}} = 0.69A_{\mathrm{opt}}^2/\lambda f. \tag{36}$$

Note that this resolving power grows with the square of the refracting aperture independently of the lens concept. It is thus identical for both Fresnel lenses with equal aperture. Equation (36) can then also be written for the CRL as

$$\lambda/\Delta\lambda\,\big|_{\mathrm{CRL}}^{\mathrm{chrom}} = 5.52\,\delta L/\lambda, \tag{37}$$

and for the Fresnel lenses as

$$\lambda/\Delta\lambda\,\big|_{\mathrm{Fresnel}}^{\mathrm{chr}} = c_{\mathrm{chr}} M_{\mathrm{Fr,opt}}\,k_{\mathrm{Fr}} = c_{\mathrm{chr}} M_{\mathrm{Cl,opt}}\,k_{\mathrm{Cl}}, \tag{38}$$

with $c_{\mathrm{chr}} = 5.52$. Interestingly these latter relations depend only on material properties for the CRLs and on the characteristic numbers M and k for the Fresnel lenses.

The finite bandwidth of the incident radiation needs to be considered at two more points. Firstly, Rayleigh's quarter-wave criterion, as discussed by Born & Wolf (1980), requests for diffraction-limited operation that the maximum distortion in the transmitted beam does not exceed an optical path difference of $\lambda/4$. We will assume all lenses to have the ideal shape. Then we can ignore the latter request for the CRLs. We have to apply this at the row borders of the Fresnel lenses, however, only after we have eventually subtracted multiples of λ at the material discontinuities.

Secondly, the maximum optical path difference has to be smaller than the longitudinal coherence length of the radiation, which is given by (Attwood, 1999)

$$l_{\mathrm{coh}} = \lambda^2/\Delta\lambda. \tag{39}$$

The optical paths at the borders of the Fresnel lenses are different from the optical paths on-axis by $N_{\mathrm{Fr}}\,m_{\mathrm{Fr}}\,k_{\mathrm{Fr}}\,\lambda$ and by $0.5\,m_{\mathrm{Cl}}^2\,k_{\mathrm{Cl}}\,\lambda$, respectively. It can then be shown that both latter

requests lead to expressions very similar to (38). However, the prefactors $c_{\mathrm{Ray}} = 2$ applicable to the Rayleigh criterion and $c_{\mathrm{coh}} = 0.5$ applicable to the longitudinal coherence length are smaller than c_{chr}. Consequently the latter two requests can be neglected compared with the resolving power required for operation free of chromatic aberrations according to (38).

2.3. Spatially coherently illuminated area

The final parameter we need to consider is the size of the spatially coherently illuminated area A_{coh} at the lens position. As X-ray sources presently do not emit radiation coherently, only a small fraction of the illuminated area at the position of the lens will contain spatially coherent radiation. For the latter area we can obtain its full width at half-maximum (FWHM) dimension, which is related to the FWHM source size S and the distance q between the source and the lens via (Attwood, 1999)

$$A_{\mathrm{coh}} = 0.44\lambda q/S. \tag{40}$$

Ideally the whole lens aperture should be illuminated spatially coherently.

3. Discussion of theoretical properties of Fresnel lenses

We will now compare the optimum geometrical apertures for Fresnel lenses with those for CRLs. The discussion will be limited to the clessidra lens; however, the properties of the standard Fresnel lenses with the same aperture can be obtained easily from the correlations discussed above.

3.1. Properties of CRLs

For CRLs the material properties can be separated in (10) from the geometrical properties in the following form, $2(2\delta L)^{1/2} = A_{\mathrm{CRL,geo}}/f^{1/2}$. The material-dependent part $2(2\delta L)^{1/2}$ is then plotted in Fig. 2 (top) for the light elements lithium, beryllium, the photoresist pmma (polymethylmethacrylate, $C_5H_8O_2$, density $1.19\,\mathrm{g\,cm^{-3}}$) and for silicon and nickel. The coordinate in this figure would be the geometrical aperture of the CRL in metres if we adjust its focal length to $f = 1\,\mathrm{m}$. We see that at larger photon energies the factor $2(2\delta L)^{1/2} = A_{\mathrm{CRL,geo}}/f^{1/2}$ approaches the same value for all materials and depends linearly on the reciprocal photon energy. At smaller photon energies the absorption starts to dominate the performance and thus the lighter elements perform better. Consequently, Be, which has been used with much success by Lengeler et al. (2004) in CRLs, is well suited as the multipurpose lens material. Lithium has already been used by Dufresne et al. (2001) but is too difficult for everyday use, while polymers, like pmma, can still provide an acceptable, cheaper and less toxic alternative.

At this point we will check the feasibility for diffraction-limited operation using such lenses. In this case the requested spectral resolving power for aberration-free operation in (37) is purely material-dependent and independent of lens properties, especially of the focal length. The minimum requested resolving power is shown in Fig. 3. The most commonly used
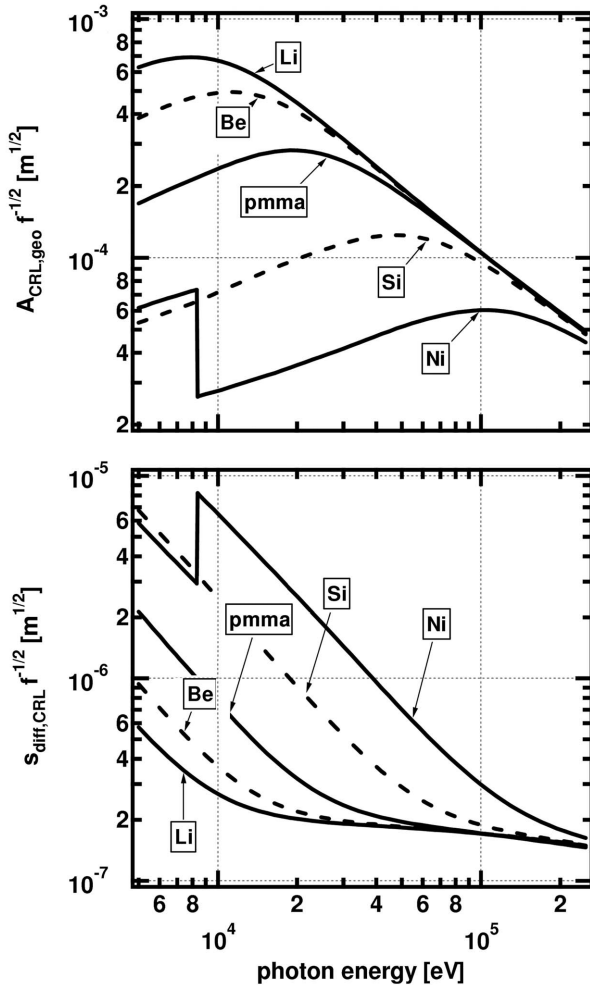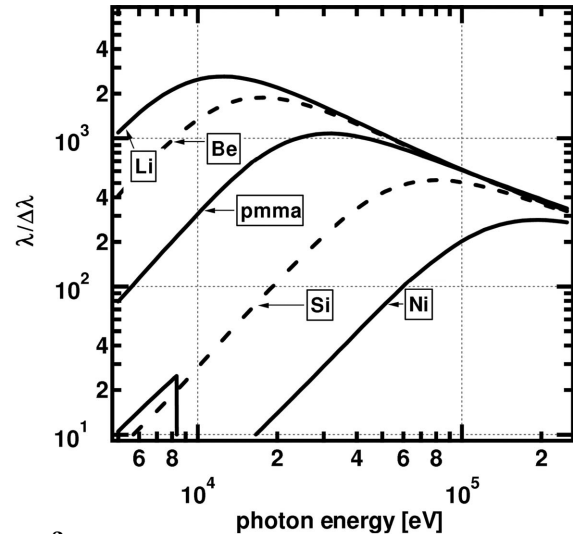
Figure 2
Top: the factor $A_{CRL,geo}/f^{1/2}$ as obtainable from (10) depending on photon energy for the materials (from top to bottom) Li, Be, pmma, Si and Ni. Bottom: the factor $s_{diff}/f^{1/2}$ depending on photon energy for the same materials. For $f = 1$ m the ordinates present the geometric apertures of compound refractive lenses $A_{CRL,geo}$ and the related spatial resolution $s_{diff,CRL}$ in both cases in metres.

monochromators at synchrotron radiation sources are double-crystal Si(111) monochromators, which can provide a spectral resolving power of at best $\lambda/\Delta\lambda \simeq 7000$. In Fig. 3 this resolving power forms the upper limit of the window. We see that it does not limit the operation of CRLs in all materials at any photon energy. In fact we can even afford a limited decrease in the spectral resolving power especially towards higher photon energy and in lenses of 'heavier' material. The related diffraction-limited spatial resolution for the CRLs can be written as

$$s_{diff,CRL} = 1.45\lambda f^{1/2}/\left[2(2\delta L)^{1/2}\right]. \qquad (41)$$

In this expression we can isolate the materials properties from the lens parameters, $s_{diff,CRL}/f^{1/2} = 1.45\lambda/\left[2(2\delta L)^{1/2}\right]$. Then the ratios for $s_{diff,CRL}/f^{1/2}$ as shown at the bottom of Fig. 2 are obtained. Here the coordinate gives directly the spatial resolution in metres for $f = 1$ m. We see that Be CRLs in particular can provide spatial resolutions in the submicrometre range

Figure 3
Spectral resolving powers according to (37) for focusing free of chromatic aberrations with CRLs depending on photon energy for the materials (from top to bottom) Li, Be, pmma, Si and Ni. The upper limit of the window corresponds to a value $\lambda/\Delta\lambda = 7000$, which is the intrinsic limitation for the resolving power of a double-crystal Si(111) monochromator.

with this focal length. As pointed out already by Schroer *et al.* (2003), the spatial resolution can be improved with shorter focal lengths at the expense of a smaller lens aperture. It can also be improved if the lens aperture follows adiabatically the decreasing beam size through a lens system (Schroer & Lengeler, 2005).

3.2. Comparison between CRLs and clessidras

At this point a few predictions can be made immediately owing to the similarities in the expressions for the apertures according to (10), (21) and (31). Indeed the dependence on the focal length is the same for all objects. Consequently, if made of the same material, a Fresnel lens will provide a larger aperture than the CRL version for $m_{Fr} = 2$ and for $m_{Cl} = 2$. Then if we consider the spectral resolving power from Fig. 3 and equation (36) we can expect some limitations on the operation of clessidras. In fact, a refractive lens with a larger aperture will not necessarily provide a better spatial resolution than the CRL if it were to replace a CRL in a beamline in which the spectral resolving power was matched to the request for the CRL. In such a case a better spatial resolution will require a monochromator providing a narrower bandwidth, which usually also means a smaller photon flux density in front of the lens.

3.2.1. Feasibility of the clessidra segment size. In order to see whether Fresnel lenses with larger apertures are really feasible, we first have to check the feasibility for Δy. A possible operation point according to (27) is obtained for $\Delta y = 10 \, \mu m$ with a focal length $f = 1$ m for $\lambda = 0.1$ nm (12.4 keV photon energy). The feature size $\Delta y = 10 \, \mu m$ is within reach only of lithographic production techniques. Now the latter process cannot shape the rotationally symmetric objects needed for bi-dimensional focusing. This requires therefore a

pair of crossed one-dimensionally focusing lenses which overlap perfectly. Then the feature depth has to be identical to the lens aperture, and the state-of-the-art in X-ray lithography for an aspect ratio a = (height A)/(width Δy) of the order of a = 100 (Nazmov *et al.*, 2000) will limit the lens aperture to the mm range. In fact, the latter can be larger than the apertures for Be CRLs. However, their combination with rather long focal lengths does not make these lenses feasible for use at X-ray laboratory sources. Nevertheless, the lenses can make good use of the characteristics of state-of-the-art synchrotron radiation sources. Indeed, the radiation from undulators is emitted into a very narrow cone such that the beam illuminates at the first optical component areas with sizes of the order of mm. Source sizes S are typically of the order of 25 μm, and the experimental stations are usually found at source distances of the order of 30–60 m. Now, an optics with focal length f will produce a demagnified image of the source with size

$$s_{\text{image}} = Sp/q = Sf/(q - f) \qquad (42)$$

if the source–lens and lens–image distances are q and p, respectively. Consequently, lenses with the discussed parameters can produce a demagnified source image of sub-micrometre size.

The feature size Δy = 10 μm is feasible according to Nazmov *et al.* (2004). However, we have to consider that sharp edges will be rounded after processing, as found by Nazmov *et al.* (2004). For example, if the sharp edges at the base of the prismatic or triangular segments in Fig. 1 are rounded to a radius of curvature of 1 μm, then the beam passing in the 2 μm adjacent to the prism bases will not be refracted as projected. This part of the radiation is not refracted to the demagnified source image and the transmitted wavefront will be distorted at the corresponding positions. Consequently the feature size of Δy = 10 μm will be considered at this point a reasonable lower limit for the production of a high-quality lens. It will lead to rather long focal lengths for larger photon energies, *e.g.* $f(E = 37\text{ keV}) = 3$ m and $f(E = 124\text{ keV}) = 10$ m. Note that shorter focal length and/or larger segment sizes are possible by using higher orders, *i.e.* $k > 1$; for example, the same feature sizes could provide half the indicated focal lengths for $k = 2$.

Having identified the possible manufacturing process, the requested segment length in the beam direction will now be investigated for the materials which are compatible with microfabrication, namely the photoresist pmma, Si and Ni. The corresponding numbers together with those for the lighter elements Li and Be are shown in Fig. 4 depending on photon energy for $p = 1$. We see that D' and Δy are of the same order of magnitude. If we now opt for rectangular prisms, *i.e.* for $D' = 2\Delta y$, the corresponding working energies are 4.3 keV for pmma lenses and 7.9 keV and 28 keV for Si and Ni lenses.

The comparison will now consider the focal lengths which are obtained from (27) for Δy = 10 μm and for $k = 1$. The predicted numbers for $A_{\text{Cl,opt}}$, which can simply be written as $A_{\text{Cl,opt}} = 2m_{\text{Cl}}\Delta y_{\text{Cl}}$, are shown in Fig. 5 for the different materials. For comparison, the aperture of a Be CRL is also presented as a dotted line in this figure. We find then that

Fresnel lenses cannot always exceed the apertures of Be CRLs. Indeed, the photon energies at which clessidras and Be CRLs have equal apertures are independent of the focal length and are 3.5 keV for pmma, 21 keV for Si and 55 keV for Ni. The two other horizontal lines in Fig. 5 are the upper aperture limits imposed by the structural parameters. First of all the already discussed state-of-the-art aspect ratio in deep X-ray lithography of a = 100 limits the aperture of the example clessidras in all materials to $A_{\text{Cl}} = a\Delta y = 100 \times 10$ μm = 1 mm
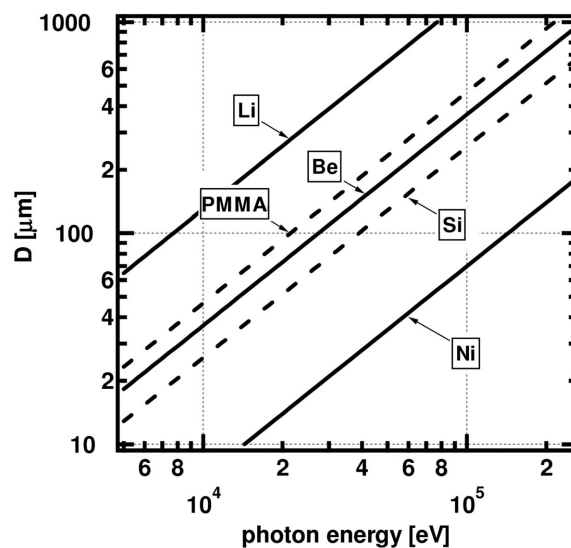
Figure 4
Material thickness D, which according to (12) will retard a passing plane wavefield by 2π in phase, depending on photon energy for the low-Z elements Li and Be and for pmma, Si and Ni.
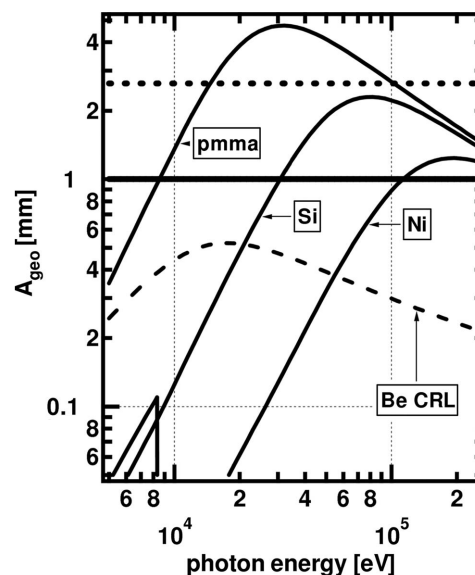
Figure 5
Optimum geometric apertures for refractive lenses depending on photon energy. The focal length is always adjusted according to (27) with a step height of Δy = 10 μm. The curves for the materials pmma, Si and Ni refer to clessidra lenses and are obtained using (30). The dashed curve refers to a Be CRL and is calculated using (10) for the same focal lengths. The thick solid line indicates the upper aperture limit of A = 1 mm for an aspect ratio of a = 100, and the dotted line is the 'thin lens' limit according to (45) for pmma clessidras.

(thick solid line). The latter is larger than the apertures of the related Be CRLs. It almost does not limit the optimum apertures of Ni Fresnel lenses, which just slightly exceed it for photon energies above 120 keV. However, especially if made from pmma, clessidra lenses could provide optimum apertures, which could significantly exceed this state-of-the-art limit for all photon energies above 8 keV. Note that the relative relations between all previously discussed curves are independent of the focal length and thus of Δy.

If we consider that the aspect ratio problem may be overcome in the future, we have to look more carefully into the geometrical shape of the Fresnel lenses. The question is then whether or not Fresnel lenses of large aperture are thin lenses.

3.2.2. Limit for 'thin lenses'. The described Fresnel lenses of highly regular shape will be operated with parameters of source distance q and source size S such that the trajectories of the incident rays are almost parallel to the row borders. Thus only a negligible amount of these trajectories would traverse these borders. Now in any prism the rays will be deflected by an angle

$$\alpha = 2\delta / \tan \gamma \qquad (43)$$

if γ is the angle of grazing incidence onto the prism side-walls. Then in the following hole these rays will be slightly displaced in the vertical direction. As these rays then accumulate angular deflections and vertical displacements in rows with many segments, they may finally impinge onto the bases of prisms in lower indexed rows. Here they will be either reflected or refracted into the adjacent row. In both cases the unpredicted additional angular deflection will deflect these rays away from the focus. Obviously this vertical displacement has no negative effect in single standard Fresnel lenses of the types in Figs. 1(c) and 1(e), and in clessidras and stacks of Fresnel lenses the rows could be bowed such that the principal trajectory of the propagating rays remains parallel to the prism bases. Schroer & Lengeler (2005) discuss this solution as adiabatically focusing Fresnel lenses. However, the present discussion will not consider this lens alternative as state-of-the-art technology cannot yet provide masks with sufficiently small features.

In row m_{Cl} of a clessidra a ray will accumulate a vertical displacement, which is approximately given by

$$\Delta Z = \alpha D' m_{Cl}^2 / 2. \qquad (44)$$

This row will no longer contribute photon flux to the focus when $\Delta Z = \Delta y$. This leads to a maximum aperture of

$$A_{\mathrm{geo,thin}} = 2(2\delta)^{1/2} f. \qquad (45)$$

It can be shown that this limit can be generally applied to Fresnel lenses, even if the number of single lenses N_{Fr} is not the optimum. Unlike in the compacted clessidras, in the standard Fresnel lenses the distance between the single lenses in the stack, w, is usually not identical to D'. If we now write $w_{Fr} = v_{Fr} N_{Fr} D'$ we finally obtain

$$A_{\mathrm{geo,thin}} = 2(2\delta/v)^{1/2} f, \qquad (46)$$

which can also be applied to correspondingly modified clessidra lenses.

In smaller lenses we have to correct the refraction efficiency of any row with the corresponding number $\Delta y - \Delta Z$. In addition, the stripe of height ΔZ will produce undesired intensity discontinuities in the transmitted wavefield. It goes beyond the scope of this report to discuss to what amount this will diffract intensity into undesired higher orders.

The dotted line in Fig. 5 now presents the 'thin lens' limit for Fresnel lenses in pmma for $v = 1$. For the other materials this limit is larger than the possible optimum apertures. However, standard Fresnel lens stacks of the types shown in Figs. 1(d) and 1(e) were previously produced with v_{Fr} varying between 2.5 and 5. Then for $v = 5$ the 'thin lens' limit is already encountered at $A = 1.7$ mm for pmma and at $A = 2.2$ mm for Si. Consequently the 'thin lens' limit is a severe limitation for pmma Fresnel lenses and it can become a limitation for lenses of other materials if a significant amount of free space is kept between the lenses in a stack. Note that this limit becomes even more severe towards smaller focal length f as the limit decreases linearly with f, while the aperture itself decreases more slowly with $f^{1/2}$.

3.2.3. Favourable operation ranges for Fresnel lenses. If we now want to assemble a bi-dimensionally focusing system from two Fresnel lenses with state-of-the-art parameters for feature size Δy and height we ideally find the following performance with respect to perfect Be CRLs. In the regions of overlap we will favour the material with the smaller D'. Then pmma Fresnel lenses provide only about twice the aperture in each direction for photon energies from 8 to 30 keV. Si Fresnel lenses provide about 2.5-fold more aperture between 30 and 80 keV, and when made of Ni these lenses provide about threefold to fivefold more aperture between 100 and 250 keV. The latter range, which is still rather unexplored with microbeams, is thus the range where state-of-the-art Fresnel lenses could present relatively the best performance. Without aspect-ratio restriction, pmma lenses could provide even tenfold more aperture than Be CRLs at around 30 keV. As far as the chromatic aberrations are concerned, we see from Fig. 3 and from (36) that the aperture increases by factors between 2 and 3 will still keep the requested monochromator resolving powers below a value of 7000, which can be provided by standard Si(111) double-crystal monochromators. Consequently these lenses could provide better spatial resolution behind this monochromator. If we then increase the aperture further, the spatial resolution will not improve any further at a given beamline. In fact, in order to utilize the spatial resolution which a pmma Fresnel lens could provide with its maximum aperture at 30 keV, one needs a monochromator resolving power of almost 200000 independently of the focal lengths. On the other hand, with resolving powers of the order of 2000, which are characteristic for uncollimated beamlines, according to (34) the presented large-aperture Fresnel lenses cannot provide submicrometre foci. This problem will not actually be encountered with achromatically focusing mirror optics, which could provide significantly smaller spots for much larger spectral bandwidth (Hignette et al., 2003; Mimura

et al., 2004). It goes beyond the scope of this study to discuss the feasibility of lens doublets for the reduction of the chromatic aberrations, as proposed by Wang *et al.* (2003).

## 4. Discussion of experimental data

4.1. Effective apertures

We will now discuss the performance of operational Fresnel lenses with experimental data obtained for clessidra lenses and with published data for standard Fresnel lenses.

4.1.1. Clessidra lenses. Several clessidra lenses were produced using a process that is explained in great detail by Pérennès *et al.* (2005). The parameter optimization was for a photon energy of 8 keV, while the lenses were then characterized systematically at a photon energy of 8.5 keV. Clessidras with state-of-the-art parameters are supposed to exceed the effective apertures of Be CRLs at these energies. Data for the first clessidra prototype with right-angle prisms ($\gamma = 45°$) and thus with $D'/\Delta y = 2$ were described earlier by Jark *et al.* (2004). This clessidra had a larger step height Δy than discussed here. The new lenses have smaller Δy with $D'/\Delta y = 3.5$ or $\gamma = 35°$. The shortest focal length of $f = 1.21$ m is then achieved for $k_{Cl} = 1$ and a step height of $\Delta y_{m,Cl} = 12.83$ μm. Such structures were produced in the photoresists pmma (lens 25/1/pmma) and SU-8 (lens 35/1/SU8). Both photoresists have identical refractive index δ, while SU-8 is slightly more absorbing than pmma, which results in $L_{SU-8} < L_{pmma}$. For comparison purposes we will include another structure (lens 35/2/pmma), which is operated in second-order $k_{Cl} = 2$ with the same angle $\gamma = 35°$. This results in a twofold larger step height of $\Delta y_{m,Cl} = 25.67$ μm for a twofold larger focal length $f = 2.42$ m. The length of all lenses in the beam direction was always $w = 2.6$ mm. The prism base widths were $D'(35/1/SU8) = 36.66$ μm, $D'(35/1/pmma) = 40.66$ μm and $D'(35/2/pmma) = 77.33$ μm, while the resist thickness was varied between 0.6 mm and 1 mm. The resultant apertures were larger than 1.3 mm.

The lens characterization was made at the SYRMEP beamline (BL6.1R, synchrotron radiation for medical physics, http://www.elettra.trieste.it/experiments/beamlines/syrmep/index.html) at ELETTRA with monochromatic synchrotron radiation of 8.5 keV photon energy and a resolving power of 2000. The lenses were always mounted at a source distance of 22.6 m from a source with a vertical height of $s = 90$ μm and a horizontal width of the order of 750 μm. High-resolution CCDs were used to register the transmission radiographs just behind the lenses and the intensity distribution in the image plane at $q = 1.28$ m and $q = 2.7$ m from the lenses, respectively. For the given experimental conditions we expect demagnified image sizes of $s_{image}(f = 2.45$ m$) = 11$ μm and $s_{image}(f = 1.21$ m$) = 5$ μm. The image broadening owing to chromatic aberrations of about 1 μm according to (34) is negligible compared with these image sizes. On the other hand, according to (40), the spatially coherently illuminated area at the lens measures only about $A_{coh} = 16$ μm. It thus covers only slightly more than one row in the lenses with $f = 1.21$ m and not even a single row in

clessidras with $f = 2.42$ m. We expect then to find in the image plane the incoherent superposition of the diffraction patterns from the single rows. It can be shown that the resulting peak is larger than the demagnified source image. In a beam with sufficient spatial coherence, clessidras would behave like linear transmission gratings. They will then produce a diffraction pattern with a peak separation in the focal plane given by $\Delta y_{m,Cl}/m$. This is smaller than the width of the incoherently produced image. The apertures of all our lenses are smaller than their corresponding 'thin lens' limits.

An example of a sequence of images taken in the systematic investigation is shown in Fig. 6 for the 35/2/pmma lens, which was produced into 0.57 mm-thick resist. Fig. 6(*a*) shows a side view of this lens taken using a macro-lens. The other pictures were taken with a high-resolution CCD camera with a nominal pixel separation of 3.9 μm. The radiograph in Fig. 6(*b*) shows the row structure of the lens, which allows us to evaluate immediately the etching depth in the holes. We can obtain the same information from the pictures in the image plane. The intensity distribution in Fig. 6(*c*) is obtained for full illumination of the lens, and that in Figs. 6(*d*) and 6(*e*) refers to windows of height 0.1 mm. In Fig. 6(*d*) this aperture illuminates the upper limit of the aperture (the bright line at the left border of the picture is the unrefracted incident beam), while
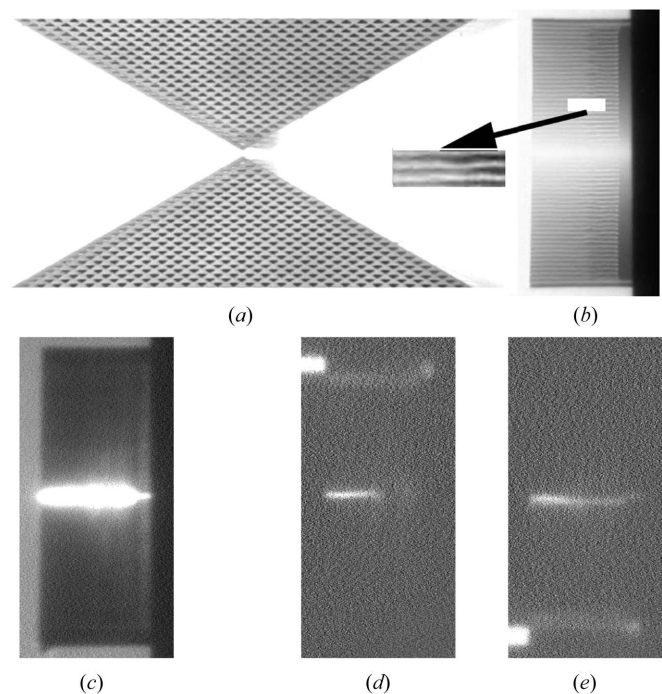
Figure 6
(*a*) Side view of the present prism lens 35/2/pmma obtained with a macro-lens. (*b*) Radiograph at 8.5 keV photon energy obtained with a CCD camera at the synchrotron radiation beamline SYRMEP at source distance $q = 22.6$ m. Part of the image in the region where the etching starts to become non-uniform is enlarged. (*c*) CCD image of the intensity distribution in the image plane of the fully illuminated lens. Note that the lens shadow is slightly larger than the lens in the radiograph in (*b*). (*d*, *e*) CCD images in the same plane obtained when an incident beam with a reduced height of 0.1 mm illuminates the upper (*d*) or the lower (*e*) lens border.
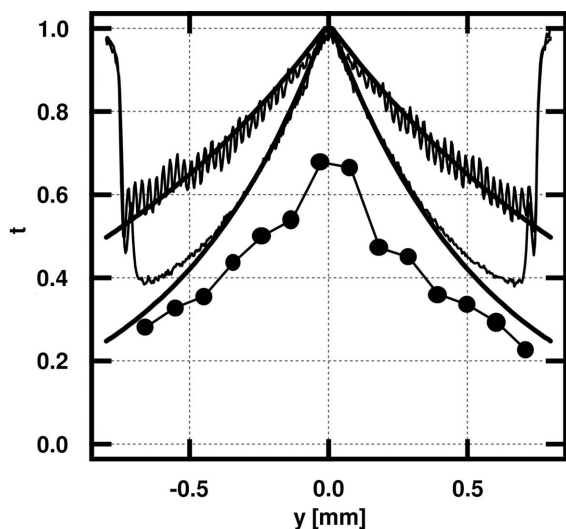
it illuminates the lower limit in Fig. 6(e). Obviously the etching is uniform for about 0.35 mm, then the channels in the radiograph start to lose straightness and the etching stops abruptly, still in the resist. In the non-uniformly etched zones the focus of the fully illuminated lens is blurred. If we use a smaller window we see that the line focus is now bent, as the non-uniformly etched zones refract the beam differently to the expectations. In the vicinity of the substrate, where no etched holes are present, the transmitted beams [weak spots at the right-hand edge of Figs. 6(d) and 6(e)] are refracted only by a small constant amount characteristic for a single large prism. From similar series of pictures we found uniform etching depths into the SU-8 resist of 0.6 mm for $\Delta y_{m,\mathrm{Cl}} = 25.67$ μm and of 0.4 mm for $\Delta y_{m,\mathrm{Cl}} = 18.34$ μm and $\Delta y_{m,\mathrm{Cl}} = 12.83$ μm. The etching process always stopped in the thicker resist. The aspect ratio is thus of the order of $a = 25$–30, i.e. significantly smaller than $a = 100$. For pmma the latter ratios were even smaller, as we find only etching depths of 0.32 mm for $\Delta y_{m,\mathrm{Cl}} = 25.67$ μm and 0.11 mm for $\Delta y_{m,\mathrm{Cl}} = 12.83$ μm. Fig. 7 reports the transmission data from the radiograph in Fig. 6(b) depending on the position y in the lens aperture. The figure contains the transmission in the etched zones (top curve) and in the unetched prismatic base (curve in centre). We find in the row structure in the data, however, that significant light scattering in the optical system between the fluorescence screen and the CCD does not allow the detection of the real signal modulation. For this discussion we will thus only calculate averaged transmission coefficients. Then the experimental data for the pmma lenses are consistent with the simulation for the transmission of a perfect prism structure with equal size for

Figure 7
Transmission t depending on position in the present prism lens as obtained from the radiograph in Fig. 6(b) and from the scan in Figs. 6(d) and 6(e). The upper oscillating curve refers to the uniformly etched area in Fig. 6(b), while the centre curve refers to a position almost in contact with the substrate. The solid lines are calculations of the transmission according to (28) using the tabulated attenuation length L and the projected amount of material in the etched zones and the underlying large prism. The dots connected by a line present the efficiency e for the beam refraction to the focus as obtained from the slit scan in Figs. 6(d) and 6(e).

the holes and the solid prisms and with the calculated attenuation length of $L = 1.62$ mm for pmma for 8.5 keV photon energy (Chantler et al., 2003). A slight overexposure of the SU-8 resist made the exposed and thus insoluble prisms larger in all directions. Then the prismatic holes in sample 35/1/SU8 have a reduced height in SEM pictures of only $\Delta y' = 9.24$ μm, while each row contains on average 70% of material instead of the projected 50%. The measured transmission of this lens in the unetched part of the lens and in the excessively filled etched zones can then be explained consistently with the shorter attenuation length of $L = 1.175$ mm. This number is consistent with that in the previous experiment (Jark et al., 2004). Note that this lens with reduced hole height $\Delta y' < \Delta y$ can at best refract 72% of the incident radiation to the focus. With the above attenuation lengths we find by use of (29) the following optimum row indices for 8.5 keV photon energy: $m_{\mathrm{Cl}}(35/1/\mathrm{pmma}) = 50$, $m_{\mathrm{Cl}}(35/2/\mathrm{pmma}) = 25$ and $m_{\mathrm{Cl}}(35/1/\mathrm{SU8}) = 36$. The corresponding optimum apertures are then 1.3 mm for pmma and 0.93 mm for SU8. Lens 35/1/pmma has just this optimum aperture, lens 35/2/pmma is slightly larger at 1.5 mm and lens 35/1/SU8 has twice the optimum aperture at 1.85 mm.

In the image plane we find experimentally at the SYRMEP beamline rather large image sizes in the vertical direction of the order of 40–60 μm for $f = 2.42$ m and slightly better values of between 35 and 50 μm for $f = 1.21$ m, and a very small signal modulation with the periodicity of the expected diffraction pattern. The image sizes remain unchanged even if we reduce the incident beam to a small line of height 0.1 mm and move it through the lens aperture. In the horizontal direction the image sizes are larger, with 70–80 μm for $f = 2.42$ m and 40 μm for $f = 1.21$ mm. These sizes are more similar to the expected demagnified source image of a horizontally larger source. For the investigation of the effective apertures and the refraction efficiency of the structures we then consider as appropriately refracted rays all those which are detected in the FWHM image size.

From the scan of the small slit which leads to Figs. 6(d) and 6(e), we can derive the experimental refraction efficiency $e(y)$. This is defined here as the relative amount of incident photon flux which is refracted into the FWHM image size. The related data for the 35/2/pmma lens are shown as the lowest curve in Fig. 7. In this lens with $\Delta y' = \Delta y$ the efficiency $e(y)$ at a given position y in the lens should ideally be identical to the average transmission of the related illuminated rows. However, the experimental data are even smaller than the transmission in the unetched part of the lens. Even in the centre of the lenses the refraction efficiency never exceeds 70%.

For the simulation of the experimental data we obviously have to consider the transmission of the rows with the material filling derived from the radiographs, $\exp[-M'(y)/L]$. In addition we will introduce a constant factor g describing the relative portion of the side-walls that refract appropriately. A misalignment in angle and a distortion of the rows will reduce the efficiency by a factor $(1 - y/l_1)$. Here l_1 is the distance from the optical axis of the lens at which a straight line of sight for parallel light no longer passes through only one row. We will

also assume that each prism will diffusely scatter intensity out of the incident intensity. This reduces the transmitted intensity to $\exp(-y/l_2)$. For small losses the latter can be approximated as $\exp(-y/l_2) \simeq (1 - y/l_2)$. Now the last two factors can be combined to $(1 - y/l_3)$, where $l_3 = l_1 l_2/(l_2 + l_1)$. The maximum error in the lens alignment would lead to $l_1 > 2.5 A$. Then we can write for the experimentally observed efficiency,

$$e(y) = g \exp[-M(y)/L][1 - (y/l_3)]. \tag{47}$$

The best description of the measured data for the lenses discussed here is presented in Fig. 8. The quality factors are then $g(35/1/SU8) = 0.6$, $g(35/1/pmma) = 0.55$ and $g(35/2/pmma) = 0.7$. Also, l_3 is always much smaller than l_1 with $l_3(35/1/SU8) = 0.85$ mm, $l_3(35/1/pmma) = 0.95$ mm and $l_3(35/2/pmma) = 2.0$ mm. This indicates that the diffuse scattering is rather significant. Indeed, the single prisms seem to scatter almost 2% of the incident intensity out of the direction to the focus. On the other hand, each prism in the SU-8 lens will absorb on average 1.56% of the incident photon flux, while for the pmma lens the corresponding numbers are 1.25% for $k = 1$ and 2.38% for $k = 2$. If the experimental value of 2% was already an ultimate limit for the scattering losses then even in a lens without absorption we find an average transmission of 0.75 for $m_{Cl} = 30$. This limits the required aspect ratio to $a = 2m_{Cl} = 60$, which is smaller than the state-of-the-art for deep X-ray lithography.
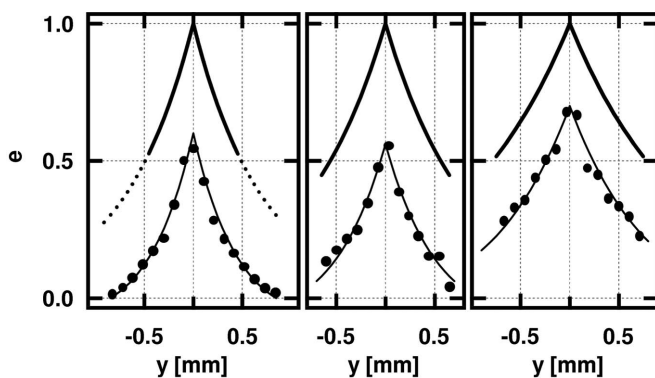
The experimental effective aperture can now be obtained in two different ways. Firstly we can determine the average experimental efficiency $\bar{e}$ within the aperture from Fig. 8 and then apply (3). Secondly we can calculate it from the properties of the image for full aperture as the product of the maximum photon flux gain G in the image and the FWHM size $s_{image,exp}$ of the image. We find here for all measured lenses from Fig. 7 that both numbers for the effective apertures coincide within experimental errors of the order of 10%.

The pmma lenses with almost optimum apertures have average refraction efficiencies of $\bar{e}$ (35/1/pmma) = 0.26 and

Figure 8
Refraction efficiency e for the focusing of X-rays depending on the off-axis position y in lenses (from left to right) 35/1/SU8, 35/1/pmma and 35/2/pmma. The dots are the measured points, the thin line is the simulation by use of (47) and the thick lines are the expected refraction efficiencies for perfect lens segments. While the solid line is the expectation inside the optimum aperture size, the dotted line refers to the prediction outside this aperture.

$\bar{e}$ (35/2/pmma) = 0.4 for expected values of 0.69 and 0.73, respectively. If we now restrict the analysis to the optimum aperture size of the SU-8 lens we obtain $\bar{e}$ (35/1/SU8) = 0.30. The outermost rows of this lens refract rather inefficiently as they were distorted in the drying process, which inclined them with respect to the optical axis of the lens. With respect to the optimum apertures the present lenses now have relative performances for the refraction efficiency of 38% (35/1/pmma), 54% (35/2/pmma) and 40% (35/1/SU8) of the expectation. The latter value would grow to 55% if we normalize the efficiency to the effectively refracting area of each row $\Delta y'/\Delta y$. So obviously the more radiation-resistant SU-8 resist is favoured over pmma for the lens material. Prismatic holes with a height of only $\Delta y' = 9.24$ μm in this resist show still high refraction efficiency, consistent with our assumption from the beginning.

As far as the effective apertures are concerned, we find $A_{eff,exp}(f = 1.21$ m$) = 0.3$ mm and $A_{eff,exp}(f = 2.42$ m$) = 0.6$ mm. The corresponding values for Be CRLs without any material on-axis according to (11) would be $A_{CRL,eff,max}(f = 1.21$ m$) = 0.48$ mm and $A_{CRL,eff,max}(f = 2.45$ m$) = 0.67$ mm. Thus our clessidras with $f = 1.21$ m lag behind this hypothetical performance, while the clessidras with about $f' = 2.42$ m could almost equal the ideal Be CRL performance.

The observations changed rather significantly when we illuminated a significant amount of the clessidras rows with spatially coherent radiation at ID22 at ESRF (Jark et al., 2004). In fact, in this case the spatially coherently illuminated area at the lens is $A_{coh} = 91$ μm for $S = 30$ μm, $q = 40$ m and for 8 keV photon energy. Then we indeed find the earlier mentioned diffraction pattern with the predicted constant peak separation in the image plane. The intensity refracted to the principal peaks was concentrated in the much smaller spot sizes of 2.8 μm, which is only slightly larger than the demagnified source image. For the principal peak we deduce an effective aperture of $A_{eff,exp} = 0.0625$ mm, which was only 17% of the expectation for the geometrical aperture $A_{geo} = 0.5$ mm used in this experiment. However, several other peaks contained very similar intensities. These intensities could actually have been concentrated into only one intense peak. This requires all phase discontinuities at the row borders to be exact multiples of 2π. In our experiment this situation could not be realised as the solid prisms contained more material than projected. Consequently Rayleigh's quarter-wave criterion could not be fulfilled at the row borders. Even though this criterion can be fulfilled with a smaller resolving power compared with the chromatic aberrations, it is a more demanding request experimentally and for lens production. It requests the tuning of the monochromator to the correct photon energy with the same relative precision. Now, the optimum photon energy cannot be predicted with a similar small error as the refractive index is not sufficiently well known and the size of the single segments cannot be repeated throughout the lens with the same tolerance. We thus expect to always find several diffraction peaks in the image plane of these lenses with large apertures.

Some comments shall be made about the operation of the presented lenses in the crossed configuration for bi-dimensional focusing, which established some of the criteria for the optimization of the structures. We built such systems from SU-8 lenses with A_{geo} = 2.62 m for f = 2.45 m and with A_{geo} = 1.85 mm for f = 1.21 m. The single lenses had experimental effective apertures of $A_{eff,exp}(f$ = 2.45 m) = 0.45 mm and $A_{eff,exp}(f$ = 1.21 m) = 0.31 mm. For the hypothetical perfect overlap of lens aperture and lens depth we then predict the experimentally expected bi-dimensional effective apertures of $A_{eff,2dim}(f'$ = 2.45 m) = 0.2 mm^2 and of $A_{eff,2dim}(f'$ = 1.21 m) = 0.096 mm^2.

Now in the experiment the etched segments from both lenses overlapped in the centre of the system for only about 0.4 mm $\times$ 0.4 mm, while the whole system was illuminated as shown in Fig. 9. From the image size $s_{image,exp}$ and the photon flux gains of $G(f$ = 2.45 m) = 26 and $G(f$ = 1.21 m) = 29 we can derive the effective bi-dimensional apertures of $A_{eff,2dim,exp}(f$ = 2.45 m) = 0.11 mm^2 and $A_{eff,2dim,exp}(f$ = 1.21 m) = 0.077 mm^2, respectively. These values are only slightly smaller than the expectation for perfectly overlapping lenses. In fact, at the position of the image we do not only find bi-dimensionally focused radiation passing in the overlapping zones of the lens; in addition we find two crossed line foci created by the radiation, which outside of the overlapping area is focused by only one of the lenses. The present simple systems thus produce foci with significant tails. Nevertheless, they are efficient beam condensers, which can only be superseded by other systems with apertures in each direction of at least 0.3 mm.

4.1.2. Standard Fresnel lenses. The experimental effective apertures $A_{eff,exp}$ for several standard Fresnel lenses can be determined from the reported data for the FWHM image size $s_{image,exp}$ and the photon flux gain G. The data and properties for lenses with reported photon flux gains G (Aristov *et al.*, 2000; Nöhammer *et al.*, 2003; Nazmov *et al.*, 2004) are presented in Table 1. Clearly neither the lens apertures A_{geo}

Figure 9
CCD image in the image plane of two crossed lenses of type 35/1/SU8 for bi-dimensional focusing. The lens apertures are 1.85 mm and the resist thickness is 0.85 mm. The white cross is the focus located 0.16 mm inside the lens. The incident unrefracted beam is light grey in colour and is found at the right and the top of the image. The lens substrates are at the left and at the bottom. The FWHM spot size measures 49 μm vertically and 54 μm horizontally and the maximum gain is G = 29.

Table 1
Data for reported standard Fresnel lenses [all lenses use p = 1 in (12)].

E = photon energy for optimization, f = corresponding focal length, A_{geo} = geometric aperture, N = number of lenses in a stacked configuration [numbers in italic are calculated by use of (16)], m = maximum row index, beamline codes refer to ESRF beamlines, S = FWHM source size, q = source–lens distance, s = measured FWHM image size, G = measured intensity increase in image, $2y_{1,Fr}$ = aperture of central segment, $y_{2,Fr} - y_{1,Fr}$ = width of first outer segment, $\Delta y_{m,Fr}$ = width of outermost segment, A_{coh} = spatially coherently illuminated lens area, $A_{CRL,eff,max}$ = ultimate effective aperture of a CRL in the same lens material according to (11). The data in empty fields are not given or cannot be derived from the provided information.

	Si†	Si†	CVD diamond‡	SU-8§	Ni¶
Reported lens properties					
E (keV)	17.0	18.0	17.5	55.2	212.0
f (mm)	800	910	1000	2000	4500
A_{geo} (μm)	150	150	500	1500	1500
N/m	5/10	5/10	12/36	*45*/140	*76*/140
Experimental conditions and results					
Beamline	BM5	ID22	BM5	?	ID15A
S (μm)	120.0	30.0	80.0		24.0
q (m)	40	62	40		45
s (μm)	2.7	2.3	3.2	8.2	5.0
G	9.1	20.3	26.0	15.4	10.0
Calculated parameters					
$2y_{1,Fr}$ (μm)	48.3	48.3	82.5	126.8	126.8
$y_{2,Fr} - y_{1,Fr}$ (μm)	10.0	10.0	17.1	26.2	26.2
$\Delta y_{m,Fr}$ (μm)	3.89	3.89	3.40	2.68	2.68
A_{coh} (μm)	10.7	62.7	15.6		4.8
$A_{eff,exp} = sG$ (μm)	24.6	46.7	83.2	126.3	50.0
$A_{CRL,eff,max}$ (μm)	73	79	300	213	92

† Aristov *et al.* (2000).   ‡ Nöhammer *et al.* (2003).   § Nazmov *et al.* (2004).   ¶ ESRF (2002).

nor the characteristic numbers for N_{Fr} and m_{Fr} were optimized according to the present scheme. Consequently we will here comment only on the feature sizes, the coherently illuminated area A_{coh} and the experimental effective apertures $A_{eff,exp}$. The lens apertures A_{geo} are such that the chromatic aberrations for a spectral bandwidth of the incident radiation of $\Delta\lambda/\lambda$ = 1/7000 should not affect the diffraction-limited resolution. None of the lenses has an aperture close to the 'thin lens' limit A_{thin}. So in principle we could expect high refraction efficiencies e. However, this is not observed. In fact the experimental effective apertures $A_{eff,exp}$ are mostly smaller and at most similar in size to the central segment $2y_{1,Fr}$. We also find in most cases that the spatially coherently illuminated area at the lens, A_{coh}, is smaller than the central segment $2y_{1,Fr}$. In some cases it is similar to the size of the first outer segment $y_{2,Fr} - y_{1,Fr}$. The incoherently illuminated central zone will, under this condition, diffract more radiation into a narrow peak in the image plane than will a spatially coherently illuminated smaller outer zone to a significantly wider peak. Consequently for the present small spatially coherently illuminated areas we expect to find in the image planes of these lenses always a central peak from which an effective aperture with the size of the central segment can be deduced. The wider diffraction peaks from the outermost zones will produce tails which will grow with increasing efficiency in these zones. The situation will change when the spatially coherently illuminated

area is larger than the central segment. Then the diffraction from several coherently illuminated outer zones can produce a peak in the image plane which has the same position and similar height and width as the peak from the central segment. We will then derive a larger effective aperture A_{eff} even for the same lens. This is exactly what we find in the experimental data obtained by Aristov *et al.* (2000) at ID22 with significantly larger spatially coherently illuminated area A_{coh}. Indeed, in this measurement the experimental effective aperture $A_{eff,exp}$ almost doubles for the same lens compared with the measurement at BM5 with a smaller spatially coherently illuminated area. Evans-Lutterodt *et al.* (2003) do not present gain data for a single lens of the type shown in Fig. 1(*c*). However, their experiment also points to the importance of the spatially coherent illumination of the lens. In fact, in this case for 12.4 keV photon energy the spatially coherently illuminated area at the lens is $A_{coh} = 71$ μm, while the lens has a slightly larger aperture of $A_{geo} = 100$ μm and a central zone of size $2y_{1,Fr} = 11$ μm. Evans-Lutterodt *et al.* (2003) measured image sizes of about $s_{image,exp} = 1$ μm, which is larger than the diffraction limit expected for the full aperture; however, it is smaller than the diffraction limit of 2 μm for the central segment. Actually this is the only case in which the measured spot size $s_{image,exp}$ corresponds to an aperture covering several internal zones. Then, in this lens, segments with sizes between $y_{2,Fr} - y_{1,Fr} = 2.3$ μm and $\Delta y_{Fr} = 0.3$ μm refracted the beam efficiently. In order to verify the efficiency of the smaller outer segments in the other Fresnel lenses at least the radiation passing the central segment would have to be blocked in the experiment. In any case we find for these lenses that their experimental effective apertures $A_{eff,exp}$ are smaller than those of easier-to-produce CRLs of the same material.

As far as clessidras are concerned, a spot size of $s_{image,exp} = 2.8$ μm (Jark *et al.*, 2004) was measured for a spatially coherently illuminated area A_{coh} covering almost five rows. The spot size is about tenfold smaller than the diffraction limit for the single rows. The experimental effective aperture $A_{eff,exp}$ corresponds to more than three rows. This effective aperture of the clessidra could even have been doubled if the diffraction pattern from the unilluminated second half of the lens had overlapped with that from the other half.

5. Conclusion

We have shown that the apertures for refractive transmission lenses of different type, *i.e.* compound refractive lenses, standard Fresnel lenses and the clessidra variant, can be compared easily in an objective way. The effective aperture A_{eff} of the latter Fresnel lenses, as a measure of the beam collection capability, can be larger than the corresponding aperture of CRLs of all materials. In the clessidra variant this is achieved in a structure which is composed essentially of small identical prisms. It is found that even structures with heights as small as $\Delta y_{Cl} = 9.24$ μm refract the X-rays efficiently. The relative performance already exceeded 50% of the ideally expected performance. These lenses presented experimental effective apertures $A_{eff,exp}$ which are very similar to the effective

apertures of perfect Be CRLs. The averaged experimental refraction efficiency is $e = 0.4$, which is already identical to the ultimately expected diffraction efficiency for linear binary zone plates (Attwood, 1999). It is shown that the lack of sufficient spatial coherence of the incident radiation can consistently explain unsatisfying small experimental gains G as well as excessively large image sizes $s_{image,exp}$ for reported Fresnel lenses of both concepts. Consequently an appreciable number of the segments in Fresnel lenses need to be illuminated spatially coherently.

Note added in proof. After the submission of the present manuscript, Cederström *et al.* (2005) published a study about another very interesting variant of the Fresnel-type X-ray lens presented here. They keep the small prisms in vertical columns and allow the vertical distance between the prism tips (referred to as d by Cederström *et al.*, 2005) in adjacent columns to be smaller than the prism height Δy (h in Cederström *et al.*, 2005). Cederström *et al.* (2005) elaborate on the two advantages of this design. First of all, the focal length f in this design can be freely adjusted and shortened independently of the prism height Δy according to $f = f_{Cl}/\gamma$, where f_{Cl} is the focal length for the clessidra design according to (27) with the same prism height Δy, and γ is defined by $\gamma = \Delta y/d \geq 1$.

Secondly, all prisms in this new prism array can be perfect prisms. Indeed, as shown by Cederström *et al.* (2005), the aberrations correction, which mandatorily has to be applied for microfocusing in the clessidra design by curving some prism side-walls, can be abandoned in their prism arrays with sufficiently small d.

The interested reader can readily obtain the relevant optical properties of a Cederström prism array from the following correlation with the present data for the clessidra lens: if we restrict γ to integer values then the position-dependent average transmission (*i.e.* the transmission function) $t(y)$ of a Cederström prism array is approximately identical to that of a stack of $N_{Cl} = \gamma$ clessidras with the same prism height Δy and the same reduced focal length $f = f_{Cl}/N_{Cl}$. For a lens stack the optimum geometrical aperture as given by (30) and (31) does then no longer depend on $f^{1/2}$ but on f. Thus the shorter focal length in the Cederström prism array is achieved at the expense of a reduced effective aperture compared with the optimum clessidra design with accordingly smaller prism height.

The experimental results for the Cederström prism array are particularly interesting as they confirm most of the lens performances for prisms of similar size elaborated here but produced by a different technique into a different material. Indeed, with a light beam which illuminates more than one prism height spatially coherently, Cederström *et al.* also observe in the lens image plane a diffraction pattern with many peaks, which are caused by the lens imperfections in the areas where the prism tips touch each other. The experimental effective apertures for focusing into the principle diffraction peak are $A_{eff,exp}(E = 13.4 \text{ keV}) = 1.4 \text{ μm} \times 39 = 54.6 \text{ μm}$ and $A_{eff,exp}(E = 14 \text{ keV}) = 2.8 \text{ μm} \times 18 = 50.4 \text{ μm}$, and are thus also in this case significantly larger than the height of the prisms

of $\Delta y = 10\ \mu m$. The total effective aperture considering all diffracted intensity is then about 135 μm in both cases for an approximately expected value of 200 μm. The latter is a very encouraging relative performance of already ∼65% of the ideally expected performance, which is even slightly better than the relative result of ∼53–55% for the clessidra lens under the same conditions presented here.

References

Aristov, V., Grigoriev, M., Kuznetsov, S., Shabelnikov, L., Yunkin, V., Weitkamp, T., Rau, C., Snigireva, I., Snigirev, A., Hoffmann, M. & Voges, E. (2000). *Appl. Phys. Lett.* **77**, 4058–4060.

Attwood, D. (1999). *Soft X-rays and Extreme Ultraviolet Radiation: Principles and Applications*, ch. 8. Cambridge University Press.

Born, M. & Wolf, E. (1980). *Principle of Optics*, 6th edition. New York: Pergamon Press.

Cederström, B., Cahn, R. N., Danielsson, M., Lundqvist, M. & Nygren, D. R. (2000). *Nature (London)*, **404**, 951.

Cederström, B., Ribbing, C. & Lundqvist, M. (2005). *J. Synchrotron Rad.* **12**, 340–344.

Chantler, C. T., Olsen, K., Dragoset, R. A., Kishore, A. R., Kotochigova, S. A. & Zucker, D. S. (2003). *X-ray Form Factor, Attenuation and Scattering Tables* (version 2.0), http://physics.nist.gov/ffast [Originally published as Chantler, C. T. (2000). *J. Phys. Chem. Ref. Data*, **29**, 597–1048; and Chantler, C. T. (1995). *J. Phys. Chem. Ref. Data*, **24**, 71–643.]

Dufresne, E. M., Arms, D. A., Clarke, R., Pereira, N. R. & Dierker, S. B. (2001). *Appl. Phys. Lett.* **79**, 4085–4087.

ESRF (2002). http://www.esrf.Fr/UsersAndScience/Publications/Highlights/2002/Methods/MET1/.

Evans-Lutterodt, K., Ablett, J. M., Stein, A., Kao, C.-C., Tennant, D. M., Klemens, F., Taylor, A., Jacobsen, C., Gammel, P. L., Huggins, H., Ustin, S., Bogart, G. & Ocola, L. (2003). *Opt. Express*, **11**, 919–926.

Henke, B. L., Gullickson, E. M. & Davis, J. C. (1993). *Atom. Data Nucl. Data Tables*, **54**, 181–342. (http://www-cxro.lbl.gov/optical_constants/.)

Hignette, O., Cloetens, P., Lee, W.-K., Ludwig, W. & Rostaing, G. (2003). *J. Phys. IV*, **104**, 231–234.

Jark, W., Pérennès, F., Matteucci, M., Mancini, L., Montanari, F., Rigon, L., Tromba, G., Somogyi, A., Tucoulou, R. & Bohic, S. (2004). *J. Synchrotron Rad.* **11**, 248–253.

Jarre, A., Fuhse, C., Ollinger, C., Seeger, J., Tucoulou, R. & Salditt, T. (2005). *Phys. Rev. Lett.* **94**, 074801.

Kirkpatrick, P. & Baez, A. (1948). *J. Opt. Soc. Am.* **38**, 766–774.

Lengeler, B., Schroer, C. G., Kuhlmann, M., Benner, B., Günzler, T. F., Kurapova, O., Somogyi, A., Snigirev, A. & Snigireva, I. (2004). *AIP Conf. Proc.* **705**, 748–751.

Lengeler, B., Schroer, C. G., Tuemmler, J., Benner, B., Richwin, M., Snigirev, A., Snigireva, I. & Drakopoulos, M. (1999). *J. Synchrotron Rad.* **6**, 1153–1167.

Michette, A. (1991). *Nature (London)*, **353**, 510.

Mimura, H., Yamauchi, K., Yamamura, K., Kubota, A., Matsuyama, S., Sano, Y., Ueno, K., Endo, K., Nishino, Y., Tamasaku, K., Yabashi, M., Ishikawa, T. & Mori, Y. (2004). *J. Synchrotron Rad.* **11**, 343–346.

Nazmov, V. P., Mezentseva, L. A., Pindyurin, V. F., Petrov, V. V. & Yakovleva, E. N. (2000). *Nucl. Instrum. Methods*, A**448**, 493–496.

Nazmov, V., Shabel'nikov, L., Pantenburg, F.-J., Mohr, J., Reznikova, E., Snigirev, A., Snigireva, I., Kouznetsov, S. & DiMichiel, M. (2004). *Nucl. Instrum. Methods*, B**217**, 409–416.

Nöhammer, B., Hoszowska, J., Freund A. K. & David, C. (2003). *J. Synchrotron Rad.* **10**, 168–171.

Pérennès, F., Matteucci, M., Jark, W. & Marmiroli, B. (2005). *Microelectron. Eng.* **78–79**, 79–87.

Schroer, C. G., Kuhlmann, M., Hunger, U. T., Günzler, T. F., Kurapova, O., Feste, S., Frehse, F., Lengeler, B., Drakopoulos, M., Somogyi, A., Simionovici, A. S., Snigirev A., Snigireva, I. & Schug, C. (2003). *Appl. Phys. Lett.* **82**, 1485–1487.

Schroer, C. G. & Lengeler, B. (2005). *Phys. Rev. Lett.* **94**, 054802.

Snigirev, A., Kohn, V., Snigireva, I. & Lengeler, B. (1996). *Nature (London)*, **384**, 49–51.

Snigireva, I., Snigirev, A., Rau, C., Weitkamp, T., Aristov, V., Grigoriev, M., Kuznetsov, S., Shabelnikov, L., Yunkin, V., Hoffmann, M. & Voges, E. (2001). *Nucl. Instrum. Methods*, A**467**, 982–985.

Suehiro, S., Miyaji, H. & Hayashi, H. (1991). *Nature (London)*, **352**, 385–386.

Tomie, T. (1994). Japanese patent 6 045288 (18 February 1994); US patent 5 594 773 (1997); German patent DE1995019505433 (1998).

Wang, Y. X., Yun, W. B. & Jacobsen, C. (2003). *Nature (London)*, **424**, 50–53.

Yang, B. X. (1993). *Nucl. Instrum. Methods*, A**328**, 578–587.

Yun, W., Lai, B., Cai, Z., Maser, J., Legnini, D., Gluskin, E., Chen, Z., Krasnoperova, A. A., Vladimirsky, Y., Cerrina, F., Di Fabrizio, E. & Gentili, M. (1999). *Rev. Sci. Instrum.* **70**, 2238–2241.